Long Term Performance Stability of Transition-Edge Sensor Detectors

S. Beaumont, J. S. Adams, S. R. Bandler, R. Borrelli, J. A. Chervenak, R. Cumbee, F. M. Finkbeiner, S. V. Hull, R. L. Kelley, C. A. Kilbourne, H. Muramatsu, F. S. Porter, K. Sakai, S. J. Smith, N. A. Wakeham, E. J. Wassell, and S. Yoon

(Invited Paper)

***Abstract*—We are developing superconducting transition-edge sensor (TES) microcalorimeter arrays for a variety of applications such as ground-based laboratory astrophysics experiments and next generation space-based X-ray missions. These detectors can provide X-ray spectral information with an unprecedent resolution of ∼2 eV at 6 keV and have for instance been selected for the X-ray Integral Field Unit (X-IFU) instrument of ESA's large flagship mission Athena. To maintain detector performance over the lifetime of the mission, it is important to understand whether environmental conditions that the detector may be exposed to will affect its properties over time. This "aging" begins right after the array leaves the fabrication environment, with potential exposure to humidity, oxygen, or elevated temperatures which may affect the detector performance. In a few prior arrays we have observed increased fall times in the pulse shape and/or the introduction of anomalous low energy tails on the X-ray spectrum. This is thought to be an indication of "aging" on chips exposed to such conditions, causing e.g., changes in the absorber properties. In this contribution, we report on a systematic characterization of TES properties, before and after exposing the chip to various controlled temperature and humidity levels and assess the changes in the measured transition and pulse shapes, energy resolution, and spectral redistribution.**

***Index Terms*—TES microcalorimeters, long term performance, low energy tail.**

Manuscript received 18 November 2022; revised 24 February 2023; accepted 27 February 2023. Date of publication 7 April 2023; date of current version 21 April 2023. The work was supported in part by NASA under Award number 80GSFC21M0002 and in part by an appointment to the NASA Goddard Space Flight Center through the NASA Postdoctoral Program, administered by Oak Ridge Associated Universities under contract with NASA. *(Corresponding author: S. Beaumont.)*

S. Beaumont, J. S. Adams, K. Sakai, and N. A. Wakeham are with the NASA Goddard Space Flight Center, Greenbelt, MD 20771 USA, and also with the University of Maryland Baltimore County, College Park, MD 21250 USA (e-mail: sbeaumon@umbc.edu).

S. R. Bandler, R. Borrelli, J. A. Chervenak, R. L. Kelley, C. A. Kilbourne, F. S. Porter, S. J. Smith, and E. J. Wassell are with the NASA Goddard Space Flight Center, Greenbelt, MD 20771 USA.

R. Cumbee is with the NASA Goddard Space Flight Center, Greenbelt, MD 20771 USA, and also with the University of Maryland College Park, College Park, MD 21250 USA.

F. M. Finkbeiner and S. Yoon are with the NASA Goddard Space Flight Center, Greenbelt, MD 20771 USA, and also with the Sigma Space Corporation, Lanham, MD 20706 USA.

H. Muramatsu is with the NASA Goddard Space Flight Center, Greenbelt, MD 20771 USA, and also with the Catholic University of America, Washington DC 20064 USA.

S. V. Hull is with the NASA Goddard Space Flight Center, Greenbelt, MD 20771 USA, and also with the NASA Postdoctoral Program, Greenbelt, MD 20771 USA.

Color versions of one or more figures in this article are available at https://doi.org/10.1109/TASC.2023.3264952.

Digital Object Identifier 10.1109/TASC.2023.3264952

I. Introduction

TRANSITION-EDGE sensor (TES) microcalorimeters are ideal when it comes to designing instruments with both imaging and high-resolution spectroscopy capabilities. These sensors are thermistors made of superconducting metals that operate in the highly temperature-sensitive transition region between the superconducting and normal metal states, providing X-ray spectral data with the exquisite resolution of ∼2 eV at 6 keV. They have hence been selected as the baseline detector technology for the X-ray Integral Field Unit (X-IFU) instrument on ESA's Athena X-ray mission [1] and for the LEM mission concept currently under development. An important aspect in the development of those detectors for such missions, or any other ground-based applications, is to make sure that they will maintain their performance over their lifetime, which include exposition to different levels of temperature or humidity from the final steps in the fabrication process all the way until their operation in space, which hence includes storage, handling, packaging, etc. This was motivated by the observation of change in the performance of detectors on a couple of occurrences, which had been exposed to uncontrolled environments leading e.g., to increased fall times in the pulse shape and/or the introduction of anomalous low energy tails on the X-ray spectrum.

In this work, we perform a systematic study of the impact of controlled humidity and temperature (separately) aiming at accelerating any performance deterioration of the detectors, characterizing the TESs before and after each exposure to assess any changes in their properties – transition shape, pulse shape, energy resolution or spectral redistribution. The humidity exposure is implemented using a dry box flushed with nitrogen gas and with petri dishes filled with water inside. The humidity level, temperature, and oxygen in the dry box are monitored using various meters. The corresponding results are described in Section III. The temperature exposure is implemented using an oven under vacuum, and the corresponding results are described in Section IV.

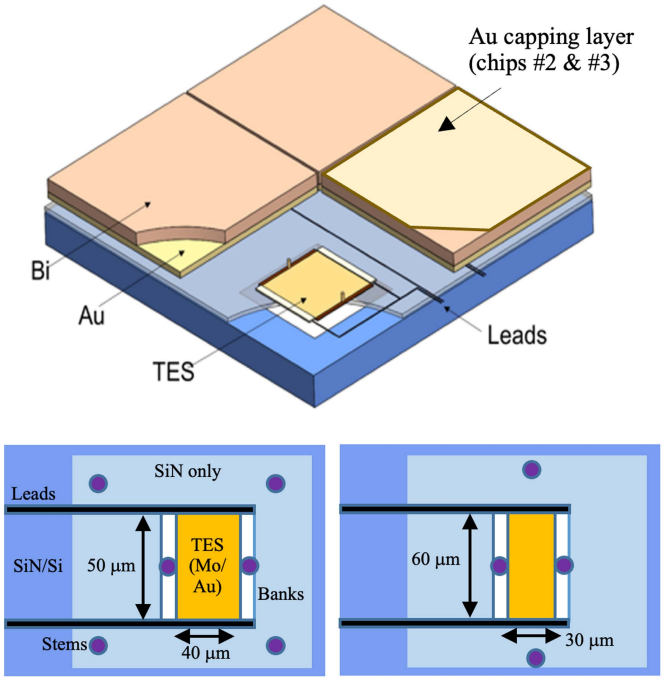

Fig. 1. (Top) simplified representation of our TES detectors in 3D. In reality, either all or none of the absorbers of a given chip have the Au capping layer. (Bottom) 2D from the top, for different TES aspect ratios and number of dotted stems. Absorbers are not shown for clarity.

TABLE I
THICKNESS OF THE BILAYERS ON EACH TEST CHIPS

Chip	Mo/Au [nm]	Bi/Au [µm]
Chip #1	47/323	3.1/1.3
Chip #2	44/240	3.1/1.3
Chip #3	46/257	5.2/1.0

II. MEASUREMENTS

A. TES Designs

The various experiments reported in this work are performed using 3 chips from different wafers, which we refer to as chip #1, chip #2, and chip #3. For all three, the TES is made of a Mo/Au bilayer deposited on a 0.5-μm-thick SiN membrane [2]. Two gold banks, parallel to the current flow, are deposited at the edges of the bilayer and on top of each of them dotted stems are used to attach the absorber. These consists of two squared electroplated layers of Au and Bi, with 275 μm side length. They are supported by 2 or 4 additional stems going to membrane, as shown on Fig. 1. The various bilayer thicknesses are reported on Table I. On each chip containing 8 $\times$ 8 TES detectors, various aspect ratios are present and were tested (50 $\times$ 40 μm^2, 60 $\times$ 30 μm^2 or 75 $\times$ 25 μm^2).

On chips #2 and #3, a second thin layer of Au was added on top of the absorbers. Such layer was initially incorporated to the design to increase the absorber's reflectivity for low energy radiations (1–20 μm wavelength range), which can cause photon shot noise [3], [4]. This is done by depositing via thermal evaporation a thin capping layer of Au of thicknesses 40 nm with a 5 nm Ti adhesion layer. As the absorbers typically have a rough surface due to the Bi grain structure, various angles are used for deposition to try and coat the surface as continuously as possible.

From the different TES designs, we measured a critical temperature Tc ranging from 65 to 90 mK, a thermal conductance of 50 to 95 pW/K at 100 mK, and a heat capacity around 0.7 pJ/K at 100 mK. The normal state resistance Rn ranges from $\sim$9–28 mΩ. Example of sensor resistance R_{TES} versus sensor temperature T_{TES} curves, for a bath temperature of 55 mK, is shown in Fig. 5. These curves are derived from measurement of the TES current as a function of the applied bias voltage (I–V), and measurement of the thermal conductance from the TES to the thermal bath Gbath. Gbath was calculated from fitting measurements of the TES Joule heating power at 0.5 Rn at various bath temperatures. Details of these measurements are described in [5], [6].

B. X-Ray Measurements

We measured several single TES devices from the 8 $\times$ 8 arrays, at a bath temperature of 55 mK and a bias point of 10% R/Rn.

Two different sources of X-rays are used, placed in turn outside the cryostat and providing X-rays with a count rate of about $\sim$1–1.5 counts per second. Those sources are an Fe-55 electron capture source, producing X-rays at 5.9 keV (Mn-Kα), and portable channel-cut crystal monochromator (CCCMs) built at GSFC [7] producing X-rays at 5.4 or 6.4 keV. A commercial Oxford X-ray tube is used to illuminate a pair of Si channel-cut crystals, aligned such that only a narrow range around the Kα_1 line of the anode material is selected – in our case Cr and Fe. Those provide gaussian lines with energy widths less than 0.5 eV FWHM, ideal to study the detector line spread function [3].

This is done by fitting the measured spectra with a normalized Gaussian function G, plus an exponential energy loss function convolved with a normalized Gaussian, F. For an incident photon energy E_i, a measured energy E, a Gaussian width σ, an energy loss fraction f and a loss strength (or length scale) s, the line shape can be described by:

$$LS(E) = (1-f)\,G(E-E_i,s) + f\,F(E-E_i,s,s).$$

III. IMPACT OF HUMIDITY

The impact of humidity was assessed using chip #1 (without Au capping layer) and chip #2 (with Au capping layer). Chip #1 was exposed to $\sim$55% humidity and then to $\sim$80% humidity, for 2 weeks each. For chip #2, smaller steps were taken at $\sim$30, 40, 50, 60 and 80% humidity, also 2 weeks at a time. We report for each chip on the impact of such exposure on the energy resolution and spectral distribution, transition shape, and pulse shape below.

A. Energy Resolution and Spectral Redistribution

Fig. 2 shows the spectra measured with the Fe CCCM X-ray source for a representative pixel on chip #1. Before any humidity exposure, the line shape presents a very small tail, with a loss

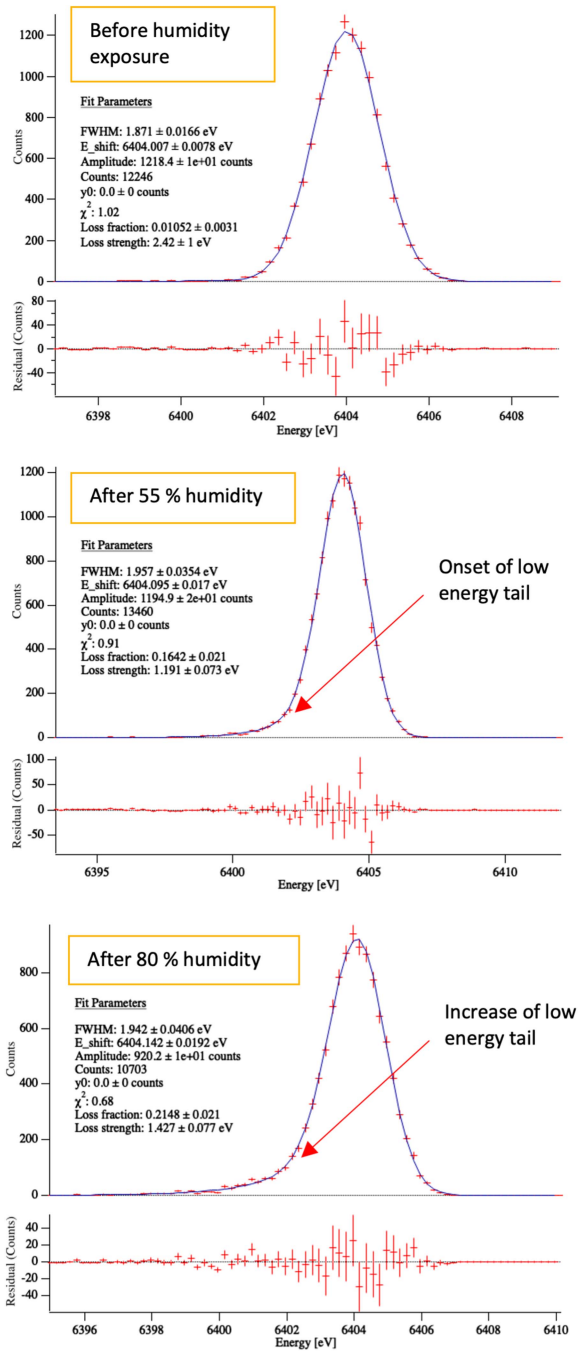

Fig. 2. Spectra measured on a pixel from chip #1 with Fe mono-chromatic source and fitted with a gaussian line shape and low energy tail. From top to bottom: Before humidity exposure, after 2 weeks at ∼55% humidity, after 2 weeks at ∼80% humidity.

fraction of ∼1%. This can be expected (even to higher level) from effects in the absorber such as electron escape or energy trapping [8]. But rather than the absolute value of the baseline level, the point of interest is how this tail evolves after different humidity exposures. After the first step, a significant increase in the size of the tail is observed, reaching 16%. A similar affect is observed after the second step, where the strength of the tail further increased to 21%. The energy resolution itself is fairly constant throughout the exposures when fitting properly with an

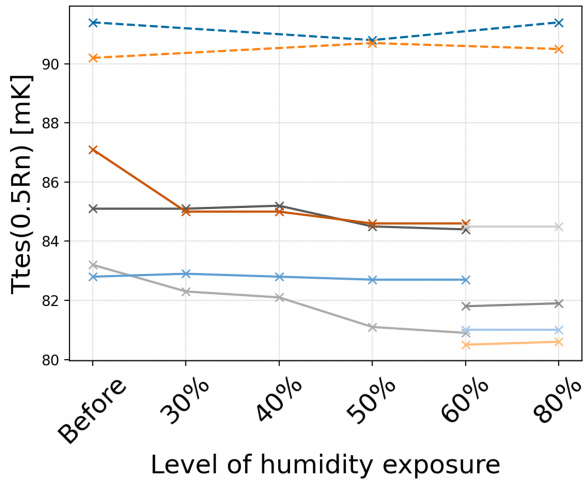

Fig. 3. TES temperature at 50% Rn for several pixels from chip #1 (dashed line) and #2 (plain line) (one color per pixel), as a function of the humidity exposure. This shows the lack of correlation between changes in the TES transitions and the humidity exposure.

energy tail, at ∼1.9 +/−0.05 eV. These observations, with an increase of the low energy after each exposure, seem to indicate an oxidation of the bismuth from the absorber with a columnar growth.

This was supported by the results from chip #2. In that case, no statistically significant change in the energy resolution or in the energy tail was measured after the different humidity exposures. The gold capping layer, although very thin, appeared to have protected the bismuth from oxidizing.

B. Transition Shapes

Throughout the humidity exposures, the transition shapes (R_{TES} vs T_{TES} curves) showed little or no variation, via small shifts in the transition temperature Tc (up to ∼2 mK), and no changes in the normal resistance or shape itself. This applies to both chip #1 and chip #2. Fig. 3 shows the shifts in transition shapes for several pixels, after the different humidity exposures. Variations appeared only for a couple pixels within the chips and did not vary steadily with the increase in humidity. They are hence thought to come from other aspects which can lead to run-to-run variations when characterizing TES detectors such as: local magnetic field not fully compensated for, change in stress locally on the membrane, change in stray power, etc, rather than a consequence of humidity.

It can be noted that a different set of pixels on chip #2 was used to check the impact of increasing humidity from 60 to 80%, due to the other pixels unfortunately being lost during manipulation of the chip.

C. Pulse Shapes

The pulse shapes also showed little to no variation from the different exposures to humidity, either for chip #1 or chip #2.

Fig. 4 shows the example for one of the pixels from chip #2 with the largest differences. One can see from the lower panel that the variation was larger after the humidity exposure

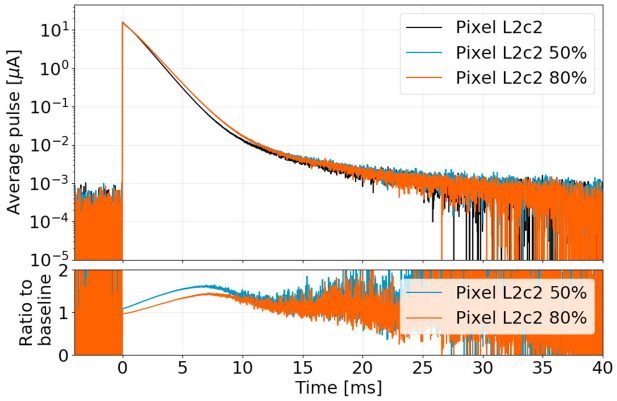

Fig. 4. Pulse shape for one pixel of chip #2 exhibiting the largest different between runs after different humidity exposure. The top panel shows the pulse themselves, and the lower panel the ratio between the pulse after a given humidity exposure and before any exposure.

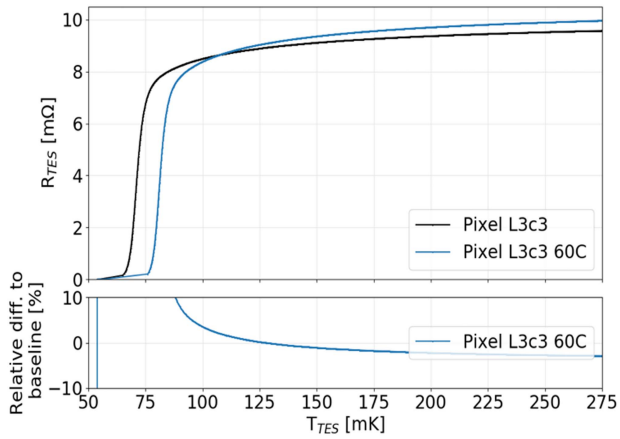

Fig. 5. Transition shapes for a representative pixel from chip #3 before and after annealing at 60 °C for 10 days, leading to an increase in both Rn and Tc.

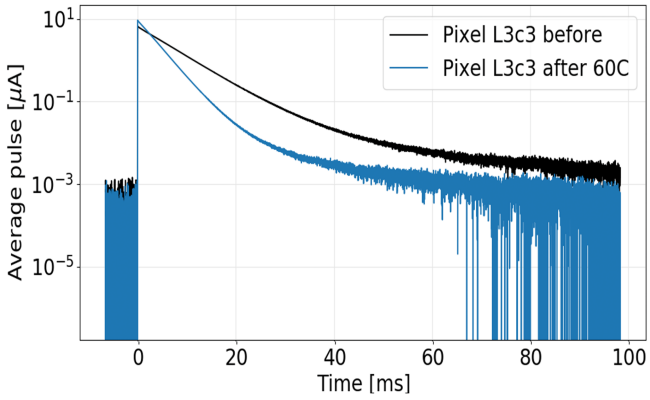

Fig. 6. Pulse shape for one pixel of chip #3, showing like the other measured detectors a large difference before and after annealing at 60 °C.

at 50% than after the one at 80%. Here again, the lack of correlation between different pixels, as well as for a given pixel between the different humidity steps, led to the conclusion that the pulse shapes were not impacted by the humidity. Rather, the differences can likely be attributed to run-to-run variations as discussed for the transition shapes.

IV. Impact of Temperature

The impact of temperature was assessed using chip #3. It was characterized before and after a single exposure to elevated temperature: 10 days at 60 °C. This value is certainly high in terms of regular storage, but was chosen as a tentatively safe high boundary, which could have covered any variation during the latest steps of fabrication such as backside heatsinking deposition (where the chip goes up to ∼68 °C for a couple hours), or at later stages during the lifetime of the detectors such as packaging, transportation, or if any bakeout at either system level was ever suggested.

A. Transition Shapes

The transition shapes before and after the high temperature exposure showed a clear change on both the normal resistance Rn and critical temperature Tc for the 4 pixels tested from chip #3. Fig. 5. shows an example for one of those pixels. We consistently observed an increase in normal resistance around 4%, and an increase in Tc between 13–19%. The increase in Tc could be measured right from the start of the characterization on the low current Tc measurements.

This change is unlikely coming from interdiffusion between the Mo and Au in the TES bilayer, since this process is only expected at much higher annealing temperatures (e.g., above 150 °C). Moreover, such process should have led to a decrease in Tc and Rn.

An increase in both those parameters rather seems to indicate a change in stress in the bilayer. Prior to the annealing, the device is under some tension from the Mo pulling on the membrane which is flexed; as it is placed at higher temperature, in a thermal expansion environment, the Mo likely releases stress in the stems, the absorbers, the membrane, or all of them, leading afterwards to more flexure and so stress in the TES. Such changes in the mechanical morphology of the film will be further investigated in the near future using visual inspections before/after annealing using a microscope and profilometer, as well as comparing TESs on membrane and on solid substrate, where we expect no change in stress with temperature.

B. Pulse Shape

As could obviously be expected following the above changes observed in the TES characteristics, the pulse shapes also appeared globally changed. Pulses after the annealing are presenting a higher pulse height and faster decay time, as shown in Fig. 6.

C. Energy Resolution and Spectral Redistribution

Again, as expected from the overall changes in the TES characteristics, the spectra before and after annealing showed some differences. It is however difficult to assess whether all of it is coming from the stress-related changes in the system, or potentially also from interdiffusion between the Bi and Au in the absorbers. This was indeed potentially expected as previous

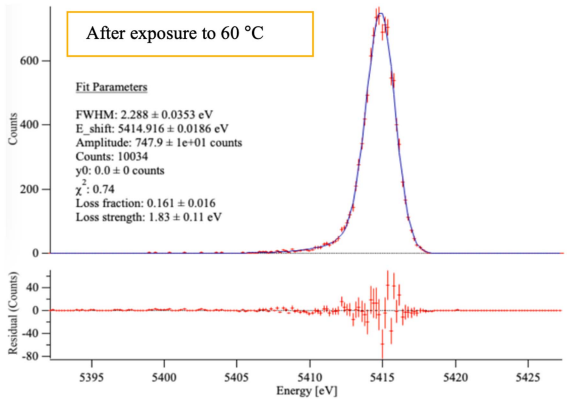

Fig. 7. Spectra measured after annealing with the Cr mono-chromatic source and fitted with a Gaussian line shape and low energy tail.

works have shown this already happening for temperature as low as 75 °C [9].

Our detectors showed a low energy tail with a fraction close to 16% even before any annealing, which as mentioned previously can be expected [8] – again, we are hence here looking at any evolution in the tail rather than its absolute value. A small increase in the low energy tail loss fraction of 0.02 eV was measured, although not statistically convincing with error bars ∼0.01 eV, as shown on Fig. 7. A follow-up inspection of the absorbers under microscope is to be done, to look visually for any changes on the absorber surface and hints of interdiffusion.

V. Conclusion

We performed a study of the impact of temperature and humidity on the long-term performance of TES detectors similar to those developed for astrophysics missions such as Athena. We observed a strong impact of the humidity on detectors with bare Bi/Au absorbers. Those appeared to oxidate, leading to an increased low energy tail on the measured spectra. After addition of a thin Au capping layer, hence protecting the Bi from oxidation, the problem appeared to have been mitigated. A confirmation test, on a chip composed at 50/50% of pixels with/without the gold capping layer and exposed to humidity as previously done will be performed in order to validate our conclusions. We also observed a strong impact from annealing the chip at 60 °C over 10 days, leading to a significant increase in Rn and Tc, and likely due to increased stress in the TES bilayer. Further investigations are scheduled to confirm the cause of the observed changes, including repeated tests with TESs on membrane versus solid substrate. Additional tests with exposures to lower temperatures and/or shorter time periods will also be performed in order to identify the starting point of the observed changes and adjust any procedure potentially affecting the TESs accordingly.

References

[1] D. Barret et al., "The athena X-ray integral field unit (X-IFU)," in *Proc. Int. Soc. Opt. Engineers Space Telescopes Instrum.: Ultraviolet Gamma Ray*, vol. 9905, 2016, Art. no. 99052F.

[2] F. M. Finkbeiner et al., "Electron-beam deposition of superconducting molybdenum thin films for the development of Mo/Au TES X-ray microcalorimeter," *IEEE Trans. Appl. Supercond.*, vol. 27, no. 4, Jun. 2017, Art. no. 2100104.

[3] M. E. Eckart et al., "Extended line spread function of TES microcalorimeters with Au/Bi," *IEEE Trans. Appl. Supercond.*, vol. 29, no. 5, Aug. 2019, Art. no. 2101205.

[4] R. Hummatov et al., "Quantum efficiency study and reflectivity enhancement of Au/Bi absorbers," *J. Low Temp. Phys.*, vol. 199, pp. 393–400, Apr. 2020.

[5] D. McCammon, "Thermal equilibrium calorimeters – an introduction," in *Cryogenic Particle Detection*, C. Enss, Ed., Berlin, Germany: Springer-Verlag, 2005, pp. 1–34.

[6] S. J. Smith et al., "Implications of weak-link behavior on the performance of Mo/Au bilayer transition-edge sensors," *J. Appl. Phys.*, vol. 114, 2013, Art. no. 074513, doi: 10.1063/1.4818917.

[7] M. A. Leutenegger et al., "Simple, compact, high-resolution monochromatic X-ray source for characterization of X-ray calorimeter arrays," *Rev. Sci. Instrum.*, vol. 91, 2020, Art. no. 083110.

[8] G. C. O'neil et al., "On low-energy tail distortions in the detector response function of X-ray microcalorimeter spectrometers," *J. Low Temp. Phys.*, vol. 199, pp. 1046–1054, 2020.

[9] J. E. Sadleir et al., "Bismuth X-ray absorber studies for TES microcalorimeters," *Nucl. Inst. Meth. Phys. Res.*, vol. 559, pp. 447–449, 2006.